Semi-analytical modelling of a multi-shaft mill

Carlos Les[a,*], James M. Finley[a], Boaz Friedland[b]

[a]*Element Digital Engineering, United Kingdom*
[b]*Energy and Densification Systems (EDS), Johannesburg, South Africa*

Abstract

Comminution is the process of breaking rock ores to extract valuable minerals and materials. The machines used to process rocks often are complex and feature many parameters which are difficult and costly to optimize. Comminution process modelling is therefore an attractive means to reduce uncertainty in comminution performance, improve energy efficiency, optimize maintenance cycles, and ultimately to deliver cost savings to manufacturers and consumers.

One way to model comminution processes is via the discrete element method (DEM), a technology which simulates the time-dependent motion of particles. However, as rocks break down into smaller pieces, the exponential growth in particle collisions can become computationally intractable. Using DEM to model full-sized comminution devices at scale is for that reason often unfeasible.

To overcome such limitation, we have developed a reduced-order mathematical model that simulates comminution processes in just minutes. The model combines physics-based breakage and mass transport models along with surrogate models trained on impact data generated from DEM simulations. This paper describes the model architecture and compares predictions of product particle size distributions with those from experiments using a multi-shaft vertical mill as a case study.

Keywords: machine learning, reduced-order modelling, discrete element method, comminution, vertical mill

*Corresponding author
Email addresses: carlos.les@element.com (Carlos Les), james.finley@element.com (James M. Finley), boaz@eds.za.com (Boaz Friedland)
URL: www.element.com/digital-engineering (Carlos Les), www.eds.za.com (Boaz Friedland)

1. Introduction

The mining industry uses comminution equipment to extract valuable materials from raw ores. Comminution often uses cutting, crushing, grinding, vibrating, and similar processes which are mechanically very intense, power hungry, and damaging to equipment. Given the enormous scale of the mining industry, small incremental improvements along the comminution process lifetime can yield very significant financial gains to manufactures and operators alike.

Research and development (R&D) of large comminution devices via iterative physical testing is typically not a viable option given the costs and slow turnovers associated with running experiments with real hardware. As a result, manufacturers and operators are incentivized to employ digital techniques to replicate and study the behaviour of real comminution hardware.

The discrete element method (DEM) is a key technology in the space of modelling and simulation of comminution processes. DEM is a numerical technique for modelling the time-dependent behaviour of bulk solids such as a large collection of rock particles. What makes DEM particularly suitable to simulating comminution devices is that the motion, impacts and breakage of particles can be modelled explicitly for each discrete particle. These features together provide a framework for high-fidelity simulations of comminution processes.

DEM is capable of modelling millions of concurrent particles. Nonetheless, the number of particles in a comminution device can surpass this number by orders of magnitude. As rocks recursively break down into finer and finer powder, the number of particles and time to compute scale exponentially. The implications are that DEM simulations of full-scale comminution processes, particularly of finer ore feeds, often become computationally intractable.

This paper presents an alternative to direct DEM simulation for modelling full-sized comminution devices in a matter of minutes. Such a significant speed-up is achieved by aggregating the motion of rocks two-dimensionally and estimating a significant portion of the recursive process of fragmenting rocks into smaller rocks via machine learning.

This piece of work seeks to demonstrate that such a semi-analytical model can be an alternative to direct DEM simulation of comminution processes. To showcase the model capabilities and use case, the paper considers a vertical multi-shaft mill from Energy & Densification Systems (EDS). The following sections describe the semi-analytical model and the reference DEM model upon which the semi-analytical model is built. Predictions of output product particle size distributions (PSDs) for the mill are then compared to experiments of processing

two different ore types: UG2, and Platreef. The paper concludes by highlighting what the semi-analytical model gets right, and the areas where it can be improved.

2. Reference discrete element method model

The EDS Multishaft Mill (MSM) selected to demonstrate the semi-analytical model is shown in Fig. 1. The EDS MSM is a compact high-velocity impact crusher comprising 5 pairs of horizontal counter-rotating rotor shafts, each spinning 18 flingers. Along with the rotors, the machine casing also encloses two outlet gates that sit below the rotor stages. The EDS MSM features an inlet chute to take in product which then refines from top to bottom (aided by gravity) via crushing, milling, densifying, blending and attrition [1], as illustrated in Fig. 2.

To ensure the semi-analytical model simulates the distribution of particles post rock fracture accurately, a machine learning model is trained on impacts data from three-dimensional DEM simulations. Importantly, these DEM simulations treat rocks as spherical particles that cannot break, which ensures they run in polynomial (rather than exponential) time—typically anywhere between $2\,\mathrm{hours}$ and $3\,\mathrm{days}$.

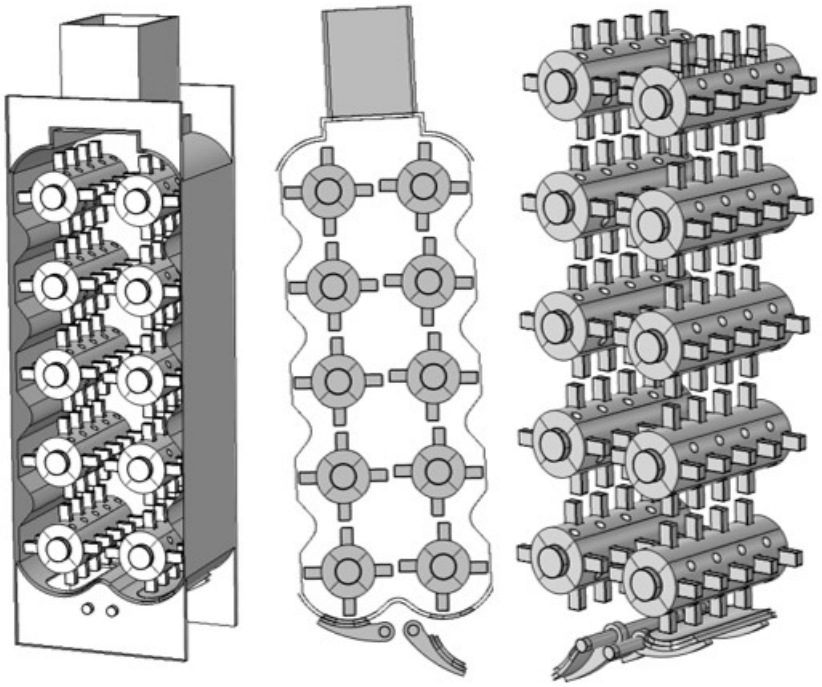

Figure 1: CAD geometry and domain of the EDS MSM in DEM simulation model.

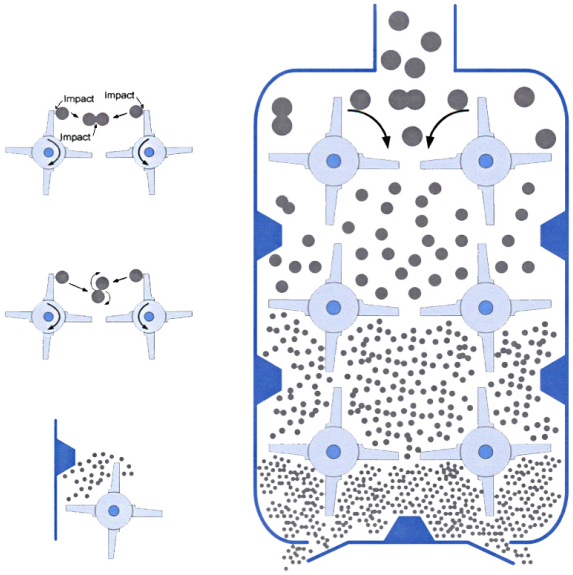

Figure 2: Schematic of high-velocity impact crushing mechanism of the EDS MSM.

The reference DEM model that simulates the time-dependent three-dimensional motion of rocks throughout the EDS MSM, from feed to machine outlet, has been developed using commercial software Rocky—now known as Ansys Rocky [2]. As Fig. 1 shows, the domain of the DEM model comprises only the EDS MSM geometry: 10 shaft rotors, flingers, casing, inlet chute, and outlet gates. The EDS MSM is modelled as a collection of surfaces that accumulate damage and wear out via deformation. Rocks are modelled exclusively as unbreakable spherical particles subject to gravity and impact forces. The contact model for particle-particle or particle-boundary collisions considers both elastic and dissipative forces to approximate the inelastic granular collisions of rocks. The size of the input particles fed from the top of the EDS MSM is defined as either a uniform distribution or a custom distribution, that way input feed experimental PSDs can be matched with ease. Different ore types are modelled by selecting appropriate material properties for the particles. Likewise, the properties for the material boundaries formed by the EDS MSM surfaces can be tuned to match those of the hardware.

Other operational settings such as the rotational direction and speed of the EDS MSM rotors, or the machine throughput (i.e. inlet mass flow rate), are varied as needed but kept constant across time. This allows a DEM simulation to model the quasi-steady state behaviour of the EDS MSM over a period of time. Typically,

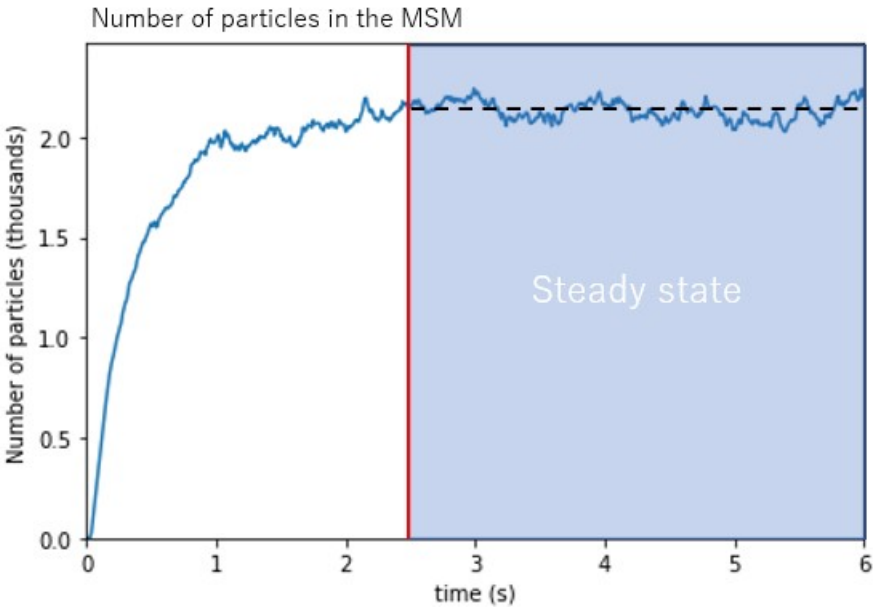

Figure 3: DEM simulation steady-state convergence.

the simulation duration is selected sufficiently long to reach steady state, which is reached once the number of particles inside the EDS MSM domain becomes stable (typically 2–3 s, as in the transient shown in Fig. 3).

The following subsections describe the governing equations that DEM solves given the constraints imposed by the normal and tangential contact force models selected. Note that in all DEM simulations, a restitution coefficient of 0.5 is used for particle-particle interactions and of 0.2 for particle-boundary interactions, and a friction coefficient of 0.4 for particle-particle contacts and 0.3 for particle-boundary contacts.

2.1. Governing equations

The motion of particles over time is determined by a set of governing equations. The time-marching scheme for each individual particle from one timestep to the next is as follows:

1. Locate all neighbouring particles and boundaries that the particle will come into contact with.
2. Calculate the sum of all forces and moments acting on the particle (Eq. (1)).
3. Move the particle to the next position based on the current timestep and the particle's current velocity and position (Eqs. (2) and (3)).

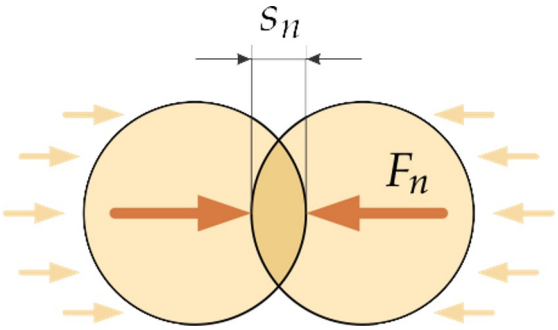

Figure 4: The normal overlap between two spherical particles.

$$\sum \mathbf{F}_{\text{net}} = \sum \mathbf{F}_{\text{body}} + \sum \mathbf{F}_{\text{surface}} = m\frac{\mathrm{d}\mathbf{v}}{\mathrm{d}t} \tag{1}$$

$$\mathbf{v}_{\text{new}} = \mathbf{v}_{\text{old}} + \frac{1}{m}\int_t^{t+\Delta t} \sum \mathbf{F}_{\text{net}}\,\mathrm{d}t \tag{2}$$

$$\mathbf{x}_{\text{new}} = \mathbf{x}_{\text{old}} + \int_t^{t+\Delta t} \mathbf{v}_{\text{new}}\,\mathrm{d}t \tag{3}$$

2.2. Normal force model

The contact model selected in Rocky's DEM simulations uses the Hertzian spring-dashpot model [3] for the normal force,

$$F_n = \hat{K}_H s_n^{3/2} + \hat{C}_H s_n^{1/4}\dot{s}_n \tag{4}$$

where $\hat{K}_H$ is the stiffness coefficient, $\hat{C}_H$ the damping coefficient, s_n the normal particle overlap as represented in Fig. 4, and $\dot{s}_n$ the relative normal velocity of particle overlap.

The stiffness coefficient,

$$\hat{K}_H = \frac{4}{3}E^*\sqrt{R^*} \tag{5}$$

is a function of the reduced Young's modulus E^* and the effective radius R^*. The Young's modulus is implicitly defined as

$$\frac{1}{E^*} = \frac{1-\nu_1^2}{E_1} + \frac{1-\nu_2^2}{E_2} \tag{6}$$

in which E_1, ν_1 and E_2, ν_2 are the Young's moduli and Poisson's ratios of the two materials in contact (for a particle-particle or particle-boundary collision). The effective radius is $L/2$ for a particle of size L in particle-boundary collision; for a particle-particle collision it is defined implicitly from the particle sizes L_1 and L_2 as follows

$$\frac{1}{R^*} = \frac{2}{L_1} + \frac{2}{L_2} \tag{7}$$

The damping coefficient,

$$\hat{C}_H = 2\eta_H \sqrt{m^* \hat{K}_H} \tag{8}$$

is a function of the damping ratio η_H for the Hertzian spring-dashpot model, and the effective mass m^*. In a particle-boundary collision, the effective mass is simply the particle mass m; in a particle-particle collision for particles masses m_1 and m_2 it is defined implicitly as

$$\frac{1}{m^*} = \frac{1}{m_1} + \frac{1}{m_2} \tag{9}$$

2.3. Tangential force model

The contact model selected in Rocky's DEM simulations uses the Mindlin-Deresiewicz model [4] for the tangential force,

$$\mathbf{F}_\tau = -\mu F_n \left(1 - \varsigma^{3/2}\right) \frac{\mathbf{s}_\tau}{|\mathbf{s}_\tau|} + \eta_\tau \sqrt{\frac{6\mu m^* F_n}{s_{\tau,\max}}} \varsigma^{1/4} \dot{\mathbf{s}}_\tau, \qquad \varsigma = 1 - \frac{\min\left(|\mathbf{s}_\tau|, s_{\tau,\max}\right)}{s_{\tau,\max}} \tag{10}$$

where μ is the friction coefficient, F_n the normal force, $\mathbf{s}_\tau$ the tangential relative displacement at the contact, $\dot{\mathbf{s}}_\tau$ the tangential relative velocity at the contact, $s_{\tau,\max}$ the maximum relative tangential displacement at which particles begin to slide, m^* the effective mass, and η_τ the tangential damping ratio.

3. Semi-analytical model

This section describes the architecture of the data-driven reduced-order model, how features are extracted from the DEM simulation data, the modelling approximations used for transport, impact and breakage of particles, and the training algorithm used to yield a complete model.

Fig. 5 gives a graphical representation of how the semi-analytical model takes in a given configuration for the EDS MSM (e.g. rotor shaft rotational speeds, gate

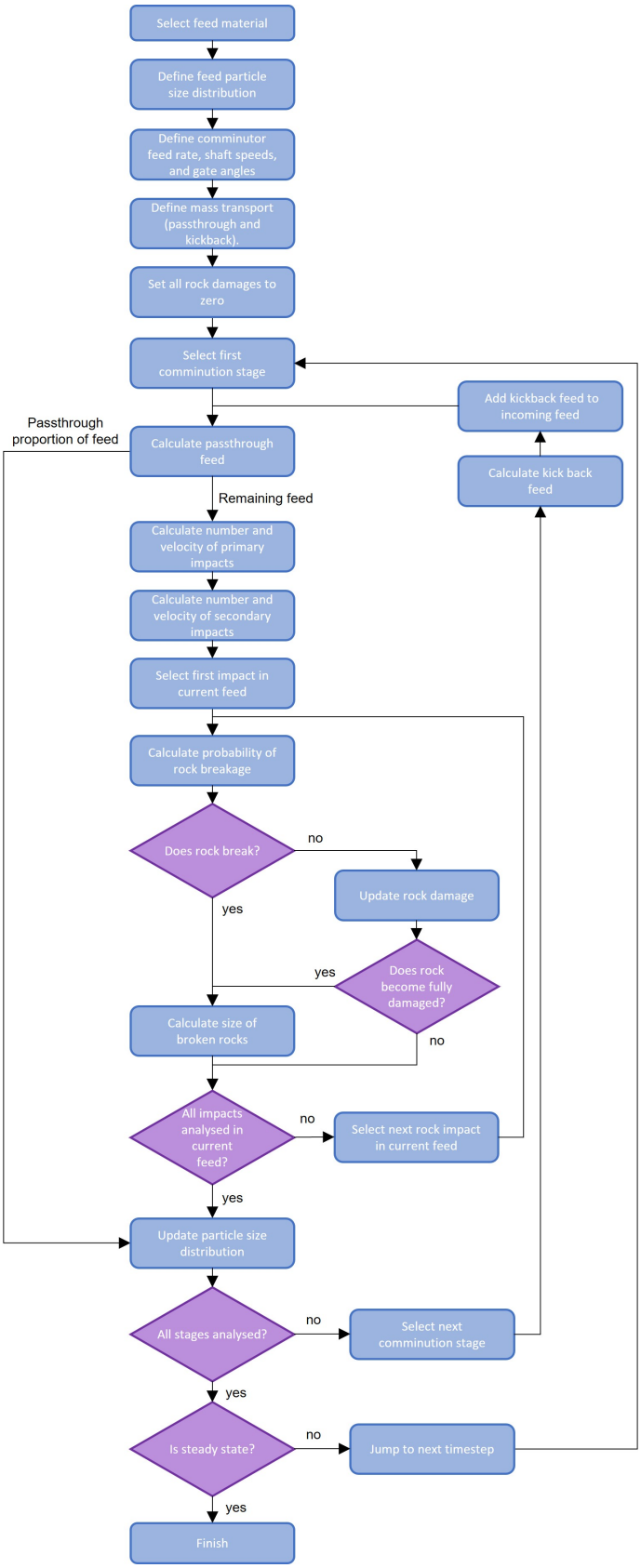

Figure 5: Flowchart of predicting the steady-state output PSD of the EDS MSM using the semi-analytical model.

angles) and operating conditions (e.g. ore type, feed rate), builds a reduced-order representation of the EDS MSM, predicts the time-dependent response of the machine, and ultimately returns a product PSD at the machine outlet. The general workflow consists of the following steps, in order of execution:

1. Select feed product (ore material, PSD, and mass flow rate).
2. Choose the EDS MSM configuration (shaft speeds and gate angles).
3. Define the mass transport model (constraints for travel of rocks).
4. Enforce that the initial state of input rocks is without defects or damage.
5. For each time step and until steady state, process rocks from inlet (top) to outlet (bottom) one stage at a time:
   (a) Calculate the transport of rocks to stages above or below.
   (b) For the rocks that remain in the current stage, compute the number and velocity of impacts.
   (c) Probabilistically determine the rocks that break or sustain damage after each impact.
   (d) After each rock fracture, compute the PSD of the resulting fragments.
   (e) Update the PSD for the current stage before proceeding to the next.

The model is built in Python and uses a set of analytical and machine learning sub-models to estimate the time-dependent mass transport, impacts, and fracture of rocks as they are processed by the EDS MSM. The following subsections describe these sub-models in detail.

3.1. Mass transport model

The mass transport through the EDS MSM is split vertically and horizontally. Rocks can travel vertically both up and down by bouncing back up to the previous stage or bypassing down to the next stage. Rocks can travel horizontally along the length of the shaft, so horizontal transport is anisotropic due to the presence of rotors. This means we require a model which captures the intricate flow of rock through the machine in both directions.

The mass transport model uses the results from the DEM model (Section 2) to analyse the movement of rock across the EDS MSM by tagging particles according to their position at specific time-steps in steady state, and tracking their motion through the EDS MSM.

To track where particles go after leaving a stage, particles are tagged in a timestep and then monitored to log the location where they move to after a characteristic time. The characteristic time is selected as the ratio of rotor stage depth to average centre velocity—$0.06\,\mathrm{s}$ in this case.

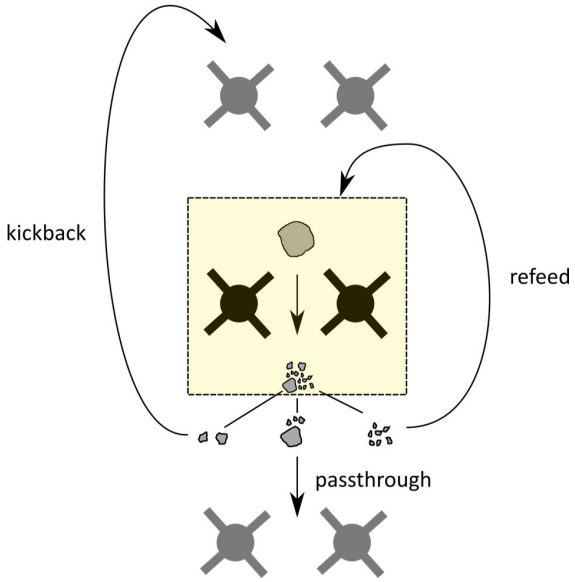

Figure 6: Schematic of particle mass transport vertical stream categories.

3.1.1. Vertical particle streams

The vertical flow is split into three major product streams: kickback (moving up), refeed (staying in stage), and pass-through (moving down). Fig. 6 shows a graphical representation of this convention. At steady state, the percentage of particles in each product stream is mostly constant. Generally, the top stage of the machine has lower material kicked back; the pass-through percentage increases with rotor speed; and the refeed percentage is lower for bigger particles.

The percentage of mass of rocks going into each vertical stream is defined by the stream percentage profile, which is determined via DEM.

3.1.2. Horizontal particle distributions

Across the horizontal rotor axes, product streams are non-uniformly distributed. The horizontal distribution of material must therefore be known to accurately capture the distribution of rock across the product streams.

We discretize the machine rotor horizontal length into 6 equidistant regions to allow for significant variation. By applying conservation principles and kinetic theory in a continuum description of the flow through the EDS MSM, the average solid volume fraction can be found. This can be used to quantify the horizontal distribution of material.

In summary, a total mass of rock going in to a stage gets distributed horizontally according to the solid volume fraction profile. The average percentage in each vertical stream coming out of the stage is then calculated as a weighted average using the solid fraction profile.

3.2. Breakage model

Rock breakage in the EDS MSM is governed by impacts suffered by the rock material as it passes through the machine. We classify impacts as being either primary or secondary. Primary impacts refer to rock-flinger collisions; secondary impacts occur as a result of non-breaking primary impacts.

A particle can only experience up to 10 primary impact events for a 5-stage EDS MSM (one for each rotor). Primary impacts are therefore deterministic and are governed purely by geometry and machine operation speed. They occur to a proportion of rocks that is determined at each stage using a mean hit probability and impact velocity calculated from the mass transport model. Secondary impacts encompass rock-liner, rock-rock, and additional rock-flinger impacts. These are modelled using separate distributions for secondary impact count and velocity gained through DEM simulations.

Both the primary and secondary impact models feed the same underlying rock breakage model by supplying an impact-specific energy. The models use a breakage model that is based upon the Ab-T10 [5] breakage model with an adaptation to capture the particle size effect inspired by [6]. This is a probabilistic model dependent on material parameters and mass-specific impact energy, which gives the breakage probability as

$$P_b = 1 - \exp\left(-bE_{cs}\frac{L}{L_{ref}}\right) \tag{11}$$

where L is the size of the parent rock and E_{cs} is the specific impact energy, $v^2/2$, where v is the relative normal velocity between rock and flinger and is determined by the flinger rotating speed.

If the rock breaks, we compute the fraction in mass of rocks below 1/10th of the initial rock mean size, known as the $t10$ value, and the resultant fragment size distribution t_n using a power-law model

$$t_n = k(t_{10})^s, \qquad t_{10} = AP_b \tag{12}$$

where k and s are constants derived from empirical data.

If the rock does not break, it accrues damage according to the Tavares damage model [7–9] and suffers secondary impacts. A rock with accumulated damage subsequently becomes more prone to suffer fracture from follow-up impacts. Damage is a dimensionless quantity ranging from 0–1, such that once damage exceeds a predefined threshold, the rock breaks.

3.2.1. Breakage calibration

The breakage model is calibrated for several ore materials and rock types. The model has three parameters which characterize the "pulverisability" A of a rock type (how much of the progeny upon breakage is below a 10th of the parent rock original size), the "breakability" b of a rock (roughly equivalent to how much energy is necessary to provoke fracture), and a "reference size" L_{ref} (which helps capture some size-dependent breakage behaviour). The parameters A and b are commonly known for many ores of interest (Table 1 shows the values for the two ores used in this study), whilst L_{ref} is not and needs calibration.

Ore	A (%)	b ($\mathrm{t}/(\mathrm{kW\,h})$)
UG2	71.8	1.67
Platreef	59	0.5358

Table 1: Parameters of the breakage model (Eqs. (11) and (12)) per ore type.

The parameters are calibrated by analysing lab-based experimental data where rocks of various sizes (covering a range of L values) are broken at various mass-specific impact energies (covering a range of E_{cs} values) and the $t10$ is measured for all cases.

3.3. Secondary impacts model

To evaluate secondary impacts, two distributions need to be known:

1. The number of impacts that take place at each rotor stage.
2. The velocity of impact events at each rotor stage.

These distributions are taken directly from the DEM simulations (see Section 2). To reduce the dimensionality of the distributions, parametric models are fitted to the two distributions for each rotor stage. A data-derived surrogate model is then trained on the fitted parameters to predict the number and velocity of secondary impacts for a variety of input conditions. The secondary impacts model fitting methodology is graphically illustrated in Fig. 7.

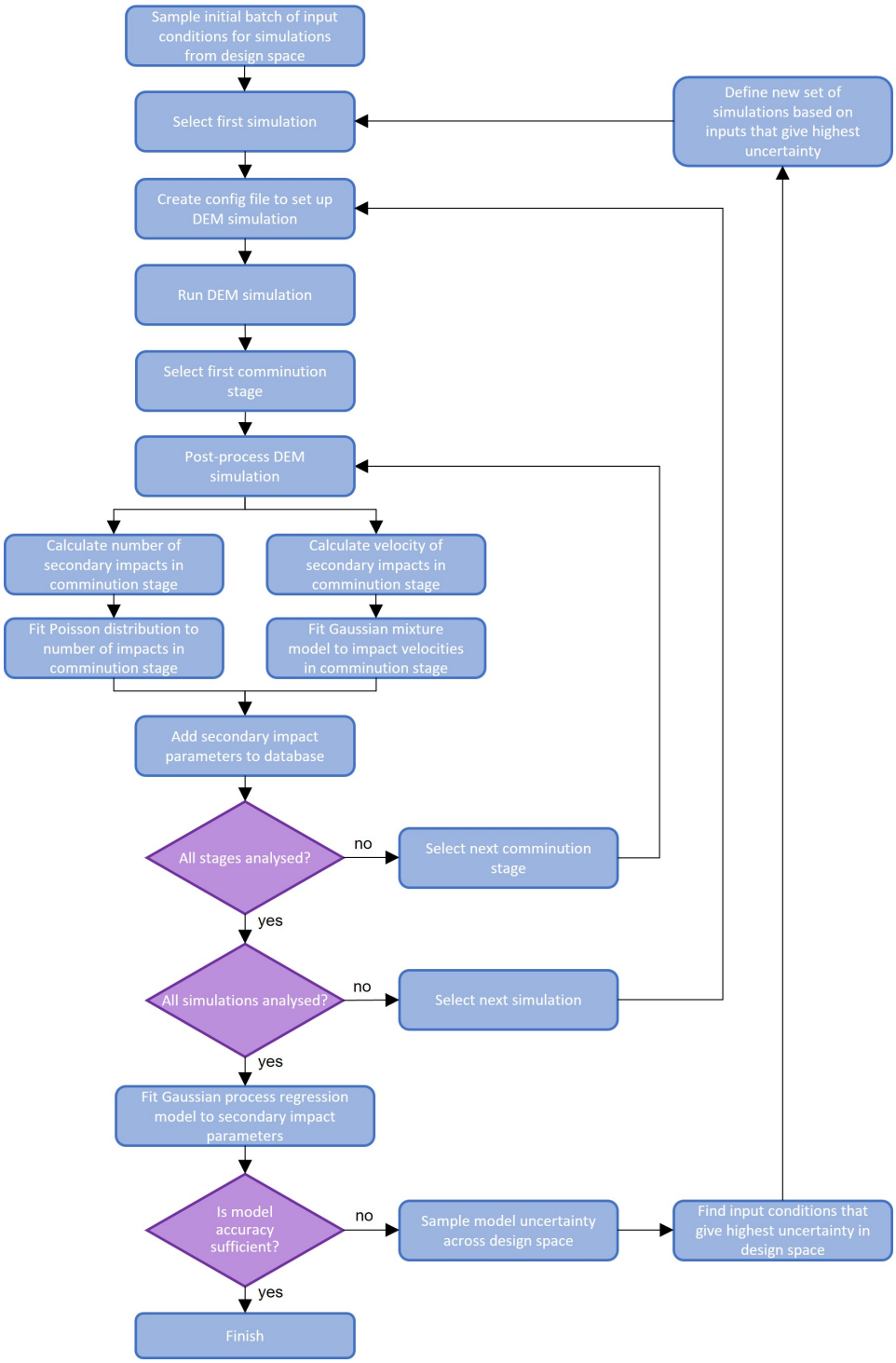

Figure 7: Flowchart of fitting the secondary impacts model to the distributions generated via DEM simulation.

3.3.1. Feature extraction

Given a non-breaking primary impact, the number of successive impacts is modelled as a Poisson distribution since it is characterizing a distribution of the number of discrete events. Therefore, at each rotor stage, we assume that the number of secondary impact events k are sampled from a Poisson distribution whose form is determined uniquely by the expected number of impacts λ,

$$p(k) = \frac{\lambda^k \exp(-\lambda)}{k!} \tag{13}$$

The secondary impact normal velocities are characterized using a Gaussian mixture model (GMM). The rationale for using this type of model is that the velocity distributions are multimodal (see e.g. Fig. 9). At each rotor stage, we fit the simulated secondary impact normal velocities to a GMM formed by K Gaussian distributions $\mathcal{N}(v|\mu_i, \sigma_i^2)$, each with their own mixture weight ϕ_i, as defined in Eq. (14). The mixture model thus has $3K$ latent parameters $(\phi_1, \mu_1, \sigma_1^2, ..., \phi_K, \mu_K, \sigma_K^2)$ that we infer from the DEM simulations.

$$p(v) = \sum_{i=1}^{i=K} \phi_i \mathcal{N}(v|\mu_i, \sigma_i^2), \qquad \sum_i \phi_i = 1 \tag{14}$$

$$\mathcal{N}(v|\mu_i, \sigma_i^2) = \frac{1}{\sigma_i \sqrt{2\pi}} \exp\left(-\frac{1}{2}\left(\frac{v-\mu_i}{\sigma_i}\right)^2\right)$$

Because the fitted distributions (Poisson and mixture of Gaussians) are highly non-linear with respect to their parameters, we use the Kullback-Leibler (KL) divergence [10, 11], Eq. (15), as a scalar measure of dissimilarity between two distributions. Minimizing the KL divergence thus yields the fit parameters for each rotor stage of each DEM simulation. Fig. 8 shows examples of the fitted distributions compared to the ground-truth distributions gathered from the DEM data.

$$D_{\mathrm{KL}}(P||Q) = \int_{-\infty}^{\infty} p(x) \ln\left(\frac{p(x)}{q(x)}\right) \mathrm{d}x \tag{15}$$

In summary, following a non-breaking primary impact, the mathematical model draws a number of secondary impacts from the Poisson distribution in Eq. (13) and a corresponding array of impact velocities from the Gaussian mixture model estimator in Eq. (14).

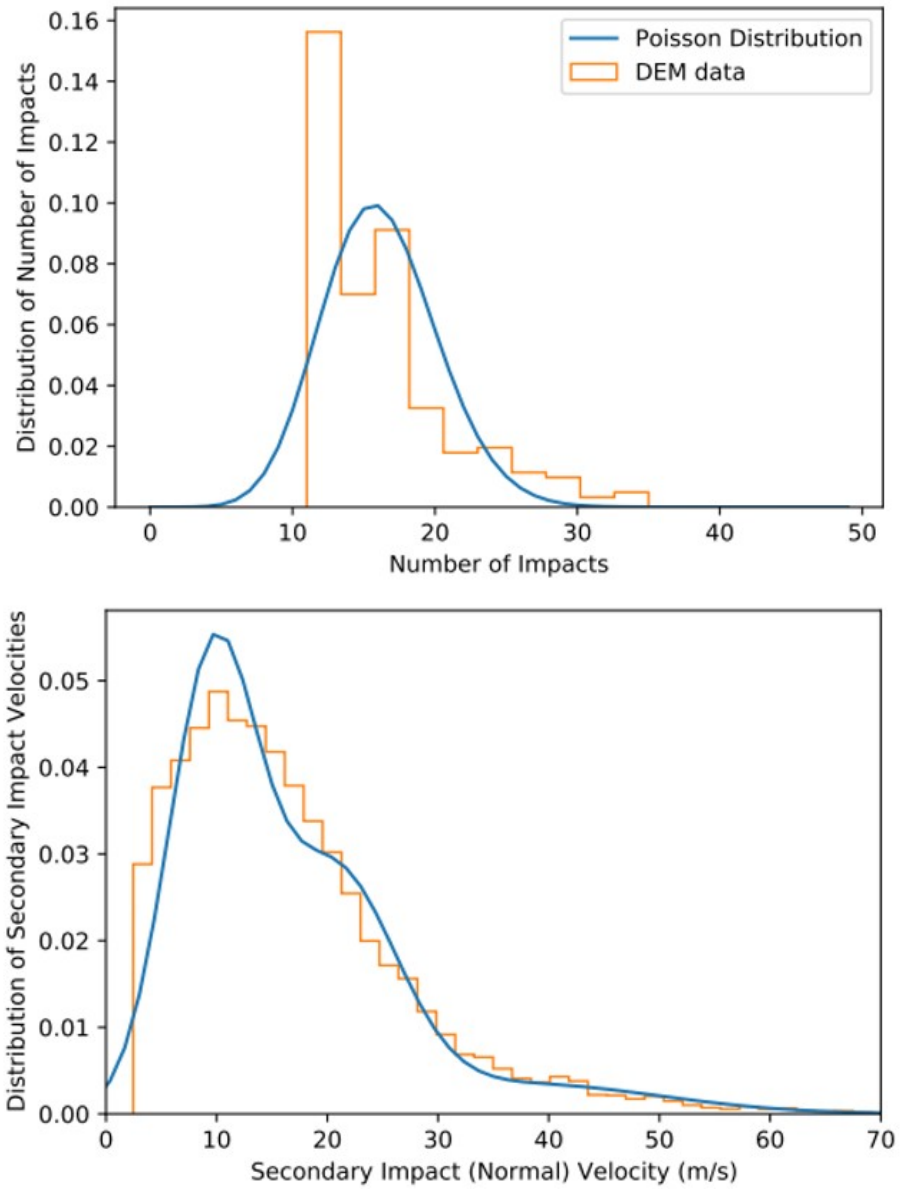

Figure 8: Comparison of DEM-generated and modelled secondary impacts distributions: (top) number of impacts from Poisson distribution, (bottom) normal velocity from Gaussian mixture model.

3.3.2. Training methodology

This subsection describes the approach taken to train a secondary impacts model that predicts how the parameters governing (i) the particle impact count distribution and (ii) the particle impact velocity distribution are influenced by different machine operating conditions.

The secondary impacts governing parameters are characterized using a Gaussian process regression (GPR) surrogate model. GPR is suitable for computationally expensive black-box functions such as our DEM simulations because it gives an indication of the predictive uncertainty of the model. This allows intelligent selection of the next training samples to minimize model uncertainty efficiently.

The GPR surrogate model uses a kernel defined by adding three kernels: ARD Matern 3/2, ARD Matern 5/2, and a white noise kernel. Matern kernels are used as they have finite differentiability, and hence can reflect real-life processes (such as impact velocities) accurately.

As the flow diagram of Fig. 7 illustrates, training of the secondary impacts GPR model is performed sequentially by sampling small batches of new DEM simulations where the model uncertainty is largest. Data from the DEM simulations of the EDS MSM in operation are processed and stored in a SQL database, which is then queried to build and train the GPR model. Once a batch of DEM simulations completes, the secondary impacts GPR model is retrained. This training loop continues until the GPR model accuracy is sufficient.

The design space for the secondary impacts GPR model is a 5-stage EDS MSM and a configuration space where for a given DEM simulation:

1. All input rocks are constrained to have the same size (unlike the semi-analytical model itself which can take any arbitrary distribution as input).
2. A constant feed rate is maintained throughout time.
3. Both outlet gates are constrained to have the same orientation.
4. All rotors in the system are constrained to have the same counter rotating speed, except for the rotors in the bottom stage which have speeds of twice the magnitude of all rotors stages above them (unlike the semi-analytical model which allows any arbitrary speed recipe).

The constraints above lead to a 4-dimensional design space ($\Re^4$). Each DEM simulation is thus defined uniquely by a 4-dimensional vector. Simulations are sampled from the domain bounded by the ranges displayed in Table 2.

In total, 177 DEM simulations have been run to train the GPR model. The mean error (KL divergence) in the GPR predictions compared to the distribution

Property	Values
Particle size	2–30 mm
Feed rate	10–60 t/h
Shaft speed	1200–1900 rad/s
Gate angle	0–80 deg

Table 2: Design space to train the secondary impacts GPR model for a 5-stage EDS MSM.

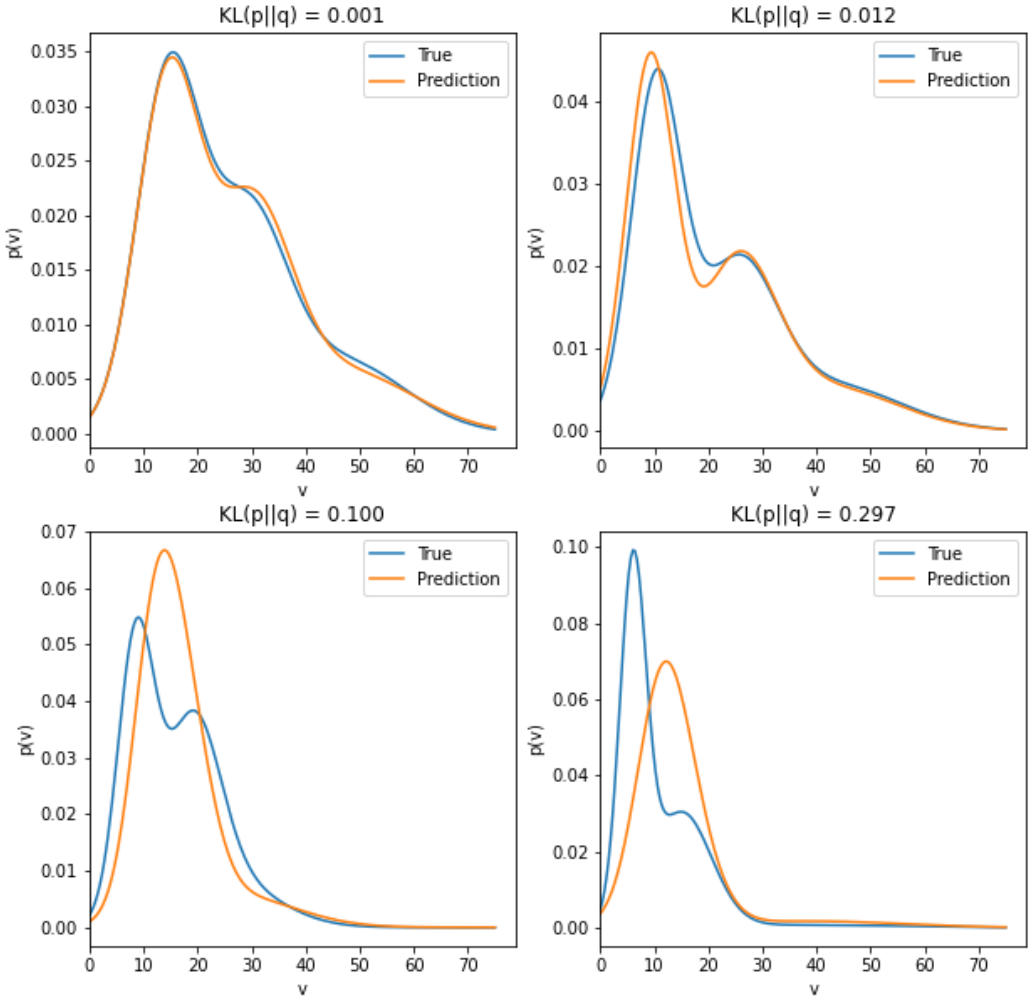

Figure 9: Kullback-Leibler (KL) divergence of a collection of velocity distributions with varying levels of accuracy. Note: the secondary impacts GPR model gives on average predictions with a K-L divergence of 0.012.

parameters previously fitted from the DEM data is 0.012. The top right subplot in Fig. 9 gives a visual representation of what a KL divergence of 0.012 corresponds to in terms of predictive accuracy for the secondary impact velocity distributions. On average, it is therefore clear that the GPR surrogate model captures the multimodal latent structure of the velocity distributions well.

4. Results

We test the semi-analytical model by performing validation runs of the EDS MSM operating at the conditions summarized in Table 3. A total of 40 comminution experiments spread across two mining sites have been used to validate the semi-analytical model: 24 performed processing UG2 ore, and 16 operated milling Platreef ore.

Property	Values
Ore material	UG2, and Platreef
Feed rate	20–50 $\mathrm{t/h}$
Shaft speed	40–65 Hz
Gate angle	40–80 deg

Table 3: Range of EDS MSM operating conditions of experiments for validation.

Fig. 10 shows the PSDs of the input rock feed supplied to the experiments running the EDS MSM. These are matched when configuring the semi-analytical model for validation. When comparing the machine output PSDs, Figs. 11 and 12 illustrate that the PSDs predicted by the semi-analytical model are consistent with those measured experimentally, across the two different sites and ore types considered. If we use the two-sample Kolmogorov-Smirnov (K-S) test as a simple proxy for prediction accuracy of the output PSDs, the semi-analytical model is able to capture the output PSDs within a K-S value of 0.07–0.18 for UG2 ore and 0.17–0.37 for Platreef ore (see Fig. 13).

Additionally, the time-dependent dynamic behaviour of the EDS MSM machine is generally preserved. For example, the time taken to reach steady state is consistent with the DEM simulations (2–3 s)—see Fig. 14 for an example of the convergence to steady state predicted by the semi-analytical model.

This demonstrates that even though the reference DEM model does not simulate breakage, the semi-analytical reduced-order model captures enough of the

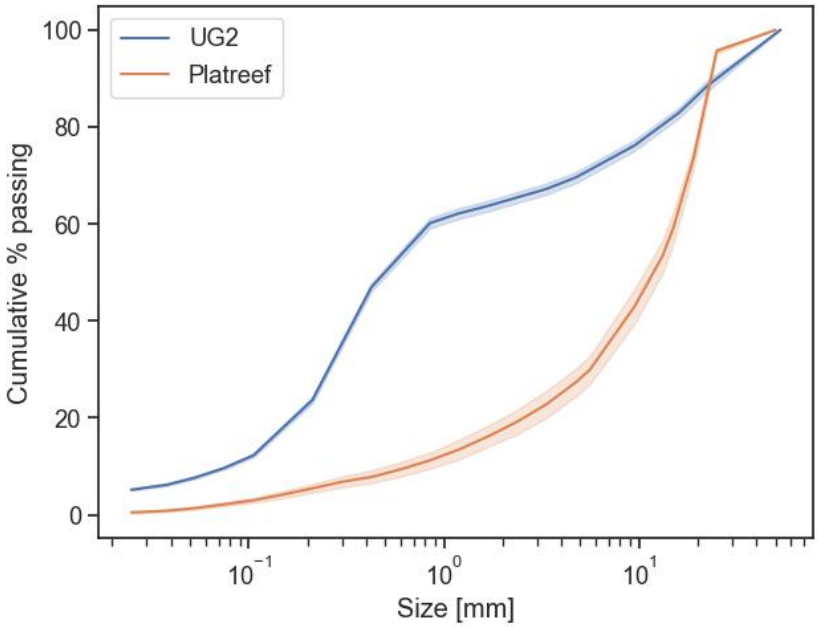

Figure 10: Mean experimental input feed particle size distributions for each ore type.

stochastic impact, fracture and mass transport mechanics to predict the machine output particle size distributions.

Looking ahead, although good predictive accuracy has been observed for the velocity and impact count distributions, further improvements could be obtained by collecting more DEM runs. More efficient improvements, however, can also be realized by improving the mass transport and breakage models since these do not require additional DEM simulations. For example, throughout this piece of work, the secondary impacts count distributions have been modelled by a monomodal Poisson distribution. In future work, our representation of this distribution could be improved by adopting a multimodal representation such as a mixture of Poissons or a constrained mixture of Gaussian distributions. Future work could additionally seek to extend the model to predict machine wear and power requirements, which would enable holistic evaluation of comminution processes.

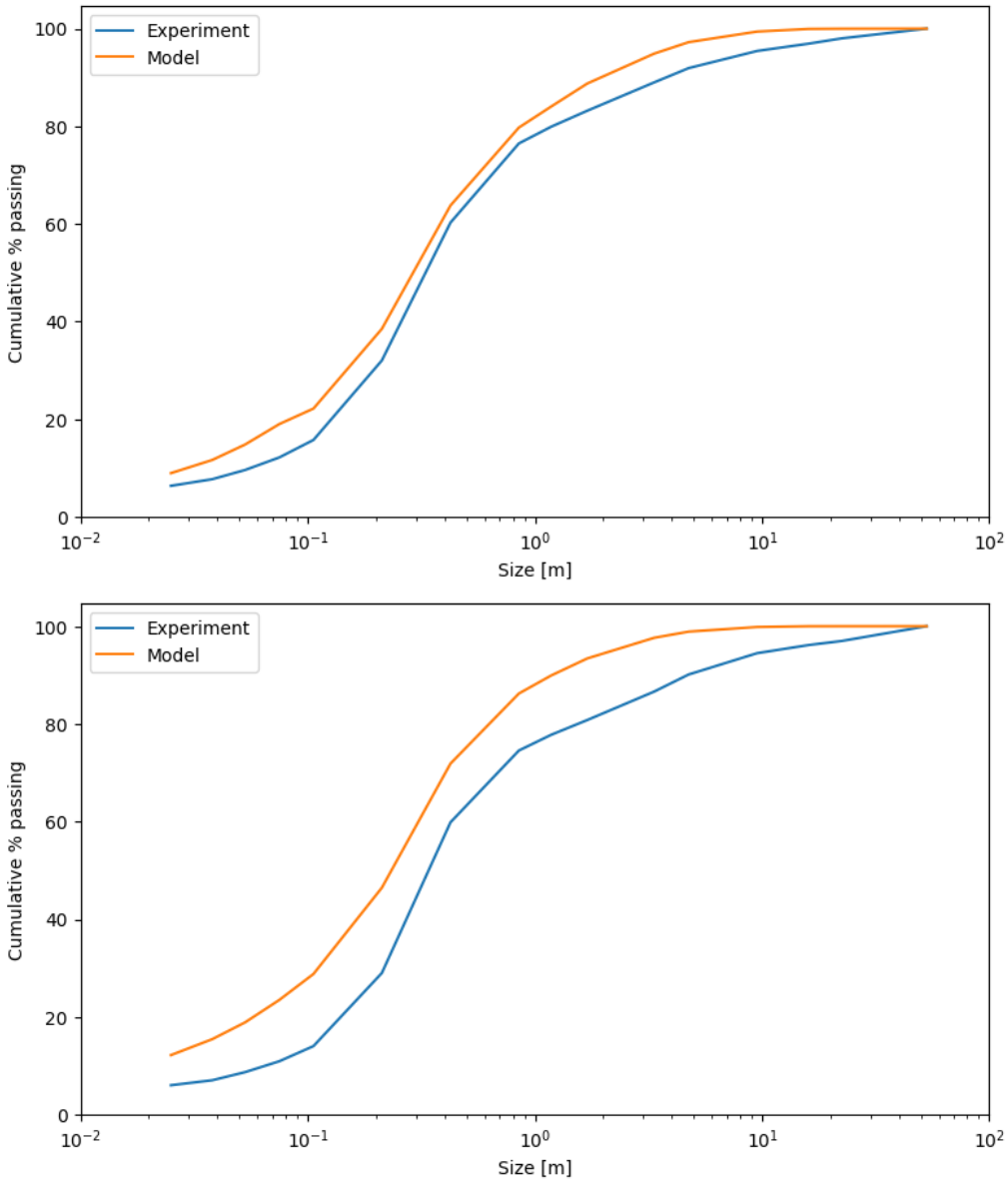

Figure 11: Comparison of experimental and modelled output PSDs for UG2 ore: (top) best prediction, (bottom) worst prediction.

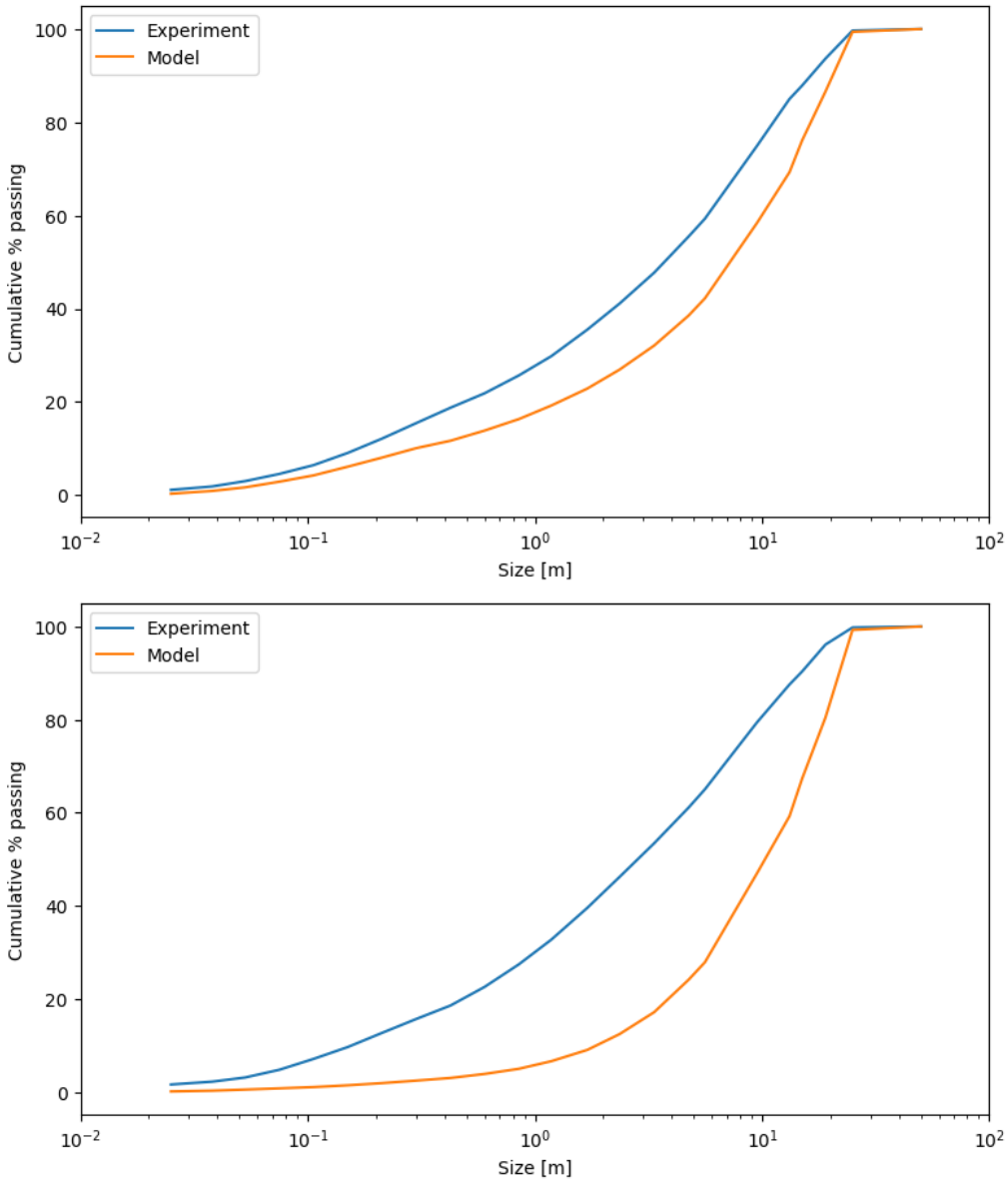

Figure 12: Comparison of experimental and modelled output PSDs for Platreef ore: (top) best prediction, (bottom) worst prediction.

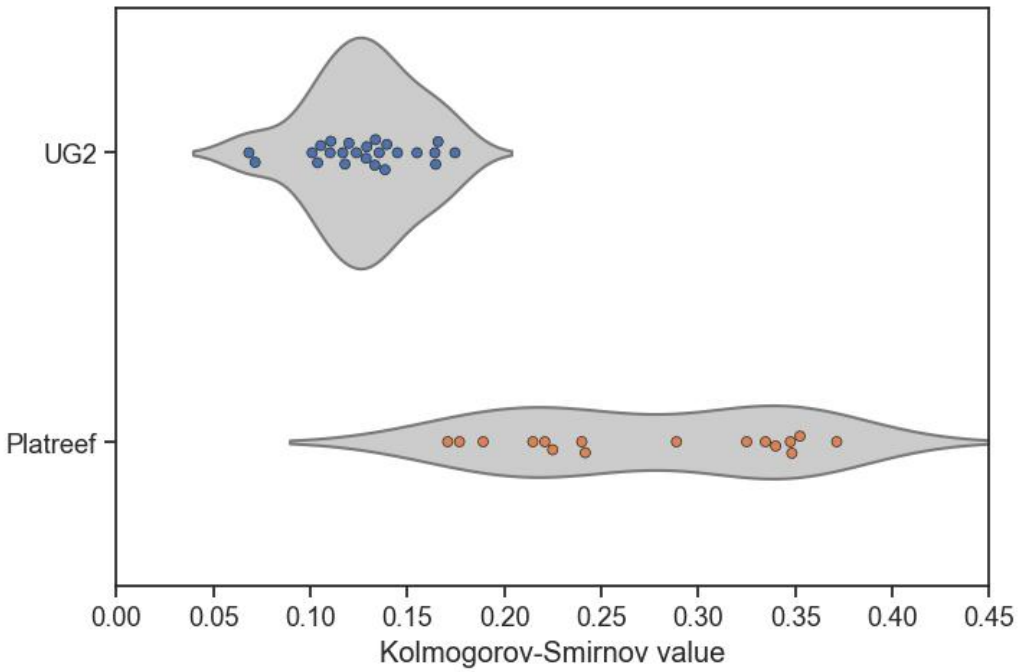

Figure 13: Swarm plot comparing Kolmogorov-Smirnov values between the experimental and predicted output PSDs of all EDS MSM experiments, for each ore type.

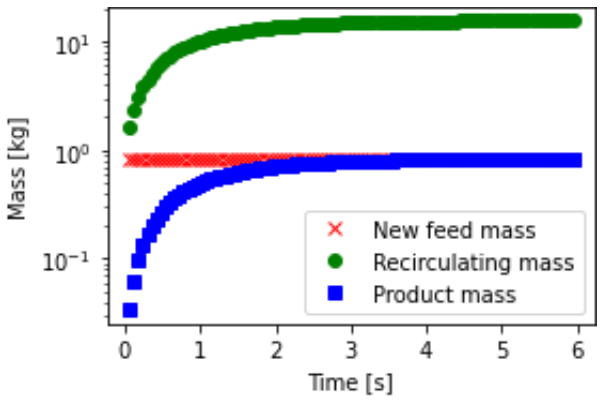

Figure 14: Example of semi-analytical model of the EDS MSM in operation reaching steady state of rock feed, recirculating mass, and product mass.

5. Conclusions

Digital simulation is an attractive vehicle for research and development of comminution technology. Amongst the modelling tools widely available, the discrete element method (DEM) arguably offers the highest fidelity when it comes to simulating rock crushing, milling or grinding. Unfortunately, because DEM treats each rock explicitly, memory and computational requirements scale exponentially as rocks recursively break down into finer and finer rocks. In other words, full-scale simulation of comminution processes down to fine powder can rapidly become computationally intractable.

Simplification of complex physics via approximations is often a workable solution to reduce the complexity of a problem. In this case, we have taken a data-driven approach to develop a semi-analytical model that simulates comminution devices in polynomial time. The model is a two-dimensional reduced-order representation built by combining analytical, probabilistic, machine learning, and DEM submodels:

- Transport of rocks is modelled in bulk, satisfying mass conservation and kinetic theory.
- Rock collisions are primarily predicted using a Gaussian process regression (GPR) surrogate model trained on impact data from three-dimensional Rocky DEM simulations of non-breaking spherical particles.
- Rock breakage is determined by a physics-informed probabilistic model which accounts for damage accumulation.

Having tested the semi-analytical model to simulate the EDS Multishaft Mill, which is a multi-shaft compact vertical mill, the following conclusions may be drawn from this piece of work:

- GPR can be trained on DEM simulation data and be used as a surrogate model to simulate the number and velocity of secondary impacts in a comminution machine.
- Narrow-scoped surrogate models such as this GPR model can be composed to form a semi-analytical model and simulate comminution processes.
- Because the training methodology of the GPR surrogate is sequential, the design space of machine operation where the GPR model is accurate can continue to be expanded by collecting more samples, i.e. more DEM simulations.

- Similarly, because the semi-analytical model is purposely architected in modular fashion, improving the fidelity of the transport or breakage of rocks along the comminution device is as simple as swapping in new modules. For example, to include the latest research in rock fracture mechanics.
- The particle size distributions of the processed product predicted by the semi-analytical model are in good agreement with those measured from a total of 40 experiments and two ore types.
- The semi-analytical model runs in a matter of minutes, making modelling of comminution processes orders of magnitude more computationally tractable than direct DEM simulation. The semi-analytical model therefore brings real value as a tool for comminution hardware design.
- Finally, whilst the semi-analytical model has been validated for particle size distributions, further work could target extensions to calculate machine wear and power requirements.

References

[1] EDS, The Multishaft Mill, Online (Mar. 2023).
URL https://www.eds.za.com/multishaft-mill/

[2] Ansys, Ansys acquires leading particle pynamics simulation software Rocky, Press release (Jan. 2023).
URL https://www.ansys.com/news-center/press-releases/1-3-23-ansys-acquires-leading-particle-dynamics-simulation-software-rocky

[3] D. Antypov, J. A. Elliott, On an analytical solution for the damped Hertzian spring, EPL (Europhysics Letters) 94 (5) (2011) 50004. doi:10.1209/0295-5075/94/50004.

[4] R. D. Mindlin, H. Deresiewicz, Elastic spheres in contact under varying oblique forces, Journal of Applied Mechanics 20 (3) (1953) 327–344. doi:10.1115/1.4010702.

[5] T. J. Napier-Munn, S. Morrell, R. D. Morrison, T. Kojovic, Mineral comminution circuits: their operation and optimisation, Julius Kruttschnitt Mineral Research Centre, 1996.

[6] L. M. Tavares, R. P. King, Single-particle fracture under impact loading, International Journal of Mineral Processing 54 (1) (1998) 1–28. doi:10.1016/s0301-7516(98)00005-2.

[7] L. M. Tavares, R. P. King, Modeling of particle fracture by repeated impacts using continuum damage mechanics, Powder Technology 123 (2-3) (2002) 138–146. doi:10.1016/s0032-5910(01)00438-7.

[8] L. M. Tavares, Analysis of particle fracture by repeated stressing as damage accumulation, Powder Technology 190 (3) (2009) 327–339. doi:10.1016/j.powtec.2008.08.011.

[9] L. M. Tavares, R. M. de Carvalho, Modeling ore degradation during handling using continuum damage mechanics, International Journal of Mineral Processing 101 (1-4) (2011) 21–27. doi:10.1016/j.minpro.2010.07.008.

[10] I. Csiszar, I-divergence geometry of probability distributions and minimization problems, The Annals of Probability 3 (1) (feb 1975). doi:10.1214/aop/1176996454.

[11] S. Kullback, R. A. Leibler, On information and sufficiency, The Annals of Mathematical Statistics 22 (1) (1951) 79–86. doi:10.1214/aoms/1177729694.